Editors' Suggestion

Resonant Plasmon-Assisted Tunneling in a Double Quantum Dot Coupled to a Quantum Hall Plasmon Resonator

Chaojing Lin,[1,2,*] Ko Futamata,[1] Takafumi Akiho,[3] Koji Muraki,[3] and Toshimasa Fujisawa[1]
[1]*Department of Physics, Tokyo Institute of Technology, 2-12-1 Ookayama, Meguro, Tokyo 152-8551, Japan*
[2]*JST, PRESTO, 4-1-8 Honcho, Kawaguchi, Saitama 332-0012, Japan*
[3]*NTT Basic Research Laboratories, NTT Corporation, 3-1 Morinosato-Wakamiya, Atsugi 243-0198, Japan*

(Received 12 October 2023; revised 30 April 2024; accepted 6 June 2024; published 15 July 2024)

Edge magnetoplasmon is an emergent chiral bosonic mode promising for studying electronic quantum optics. While the plasmon transport has been investigated with various techniques for decades, its coupling to a mesoscopic device remained unexplored. Here, we demonstrate the coupling between a single plasmon mode in a quantum Hall plasmon resonator and a double quantum dot (DQD). Resonant plasmon-assisted tunneling is observed in the DQD through absorbing or emitting plasmons stored in the resonator. By using the DQD as a spectrometer, the plasmon energy and the coupling strength are evaluated, which can be controlled by changing the electrostatic environment of the quantum Hall edge. The observed plasmon-electron coupling encourages us for studying strong coupling regimes of plasmonic cavity quantum electrodynamics.

DOI: 10.1103/PhysRevLett.133.036301

Quantum Hall (QH) edge channels provide unique opportunities for studying electronic quantum optics under strong Coulomb interactions in two complementary regimes [1–3]. In the single-electron transport regime with flying electrons well isolated from the cold Fermi sea, the Coulomb repulsion between flying electrons induces correlated single-electron transport, as demonstrated in two-particle interferometry and quantum tomography experiments [4–13]. This potentially provides a mechanism for correlated quantum state transport from one functional device to another. In the plasmon transport regime with collective motion of the cold Fermi sea, the Coulomb interaction plays an essential role in formation of emergent bosonic modes from fermions, such as edge magnetoplasmon modes and Tomonaga-Luttinger liquids [14–22]. While the classical wave nature of edge plasmons is clearly resolved, for example, with plasmon resonators and interferometers [23–26], the quantum plasmon mode is revealed recently [27]. Application of these electronic modes in either regime to a mesoscopic functional device should pave the way for exploring electronic quantum optics in QH systems known as a 2D topological insulator.

The edge plasmons have several advantages for this direction. Thanks to the chirality of the QH system, plasmons as well as flying electrons travel unidirectionally without showing backscattering [22]. The plasmon wavelength (about 100 μm at frequency of 4 GHz) is convenient for confining plasmons in a small region [24,28]. Of particular interest is the high impedance Z of the plasmon mode [29], which provides large voltage amplitude ($\tilde{V} \simeq \sqrt{Zhf}$) for a given plasmon energy (hf). This is attractive for making a strong electric dipole coupling to external atoms or qubits with the scheme of cavity quantum electrodynamics (cQED) [30,31]. Remarkably, $Z = h/\nu e^2$ is quantized as a result of the topological state. One can reach significantly large Z with small Landau-level filling factor $\nu = 2, 1, 1/3\ldots$, as compared to the impedance of the vacuum ($\simeq$377 Ω) and state-of-the-art high-impedance transmission lines made of a Josephson junction array (a few kilohms) [32–34]. Therefore, the edge plasmons are attractive for studying the strong, ultrastrong, and deep-strong coupling regimes of plasmonic cQED systems [35]. These fascinating characteristics have stimulated theoretical proposals, such as long-range entanglement [36]. However, experimental handling of chiral plasmons remains challenging.

Here, we exploit a coupled plasmon-electron system, in which an on-chip QH plasmon resonator is capacitively coupled to a double quantum dot (DQD). Discrete resonant frequencies of the resonator manifest the wave nature of plasmons, and the resonance allows us to access a single plasmon mode with a fixed energy. The coupling induced resonant plasmon-assisted tunneling (PlAT) in the DQD is observed, where the tunneling is allowed by absorption and emission of single or multiple plasmons. We clarify the plasmon-electron coupling based on the unique frequency and magnetic-field dependence of the PlAT. Some prospects for cQED applications are described. These results encourage us to study strong coupling regimes.

We propose and demonstrate a novel hybrid system consisting of a plasmon resonator in an isolated circular QH region and a charge two-level system (TLS) in a DQD, as shown in Fig. 1. The device was fabricated in a GaAs/AlGaAs heterostructure with a 2D electron gas

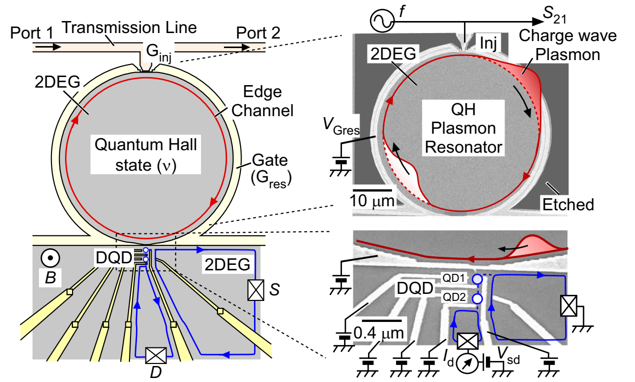

FIG. 1. Schematic of the device (left) and SEM pictures of the plasmon resonator (upper right) and the DQD (lower right). The plasmon resonator is formed as a circular QH channel propagating along the inner edge of the ring-shaped gate electrode G_{res}. The upper half of the 2DEG outside the resonator (the black region in the upper SEM) has been removed by wet etching. The resonant mode is represented by wave packets with excess and deficit charges. A gate defined DQD (the two small circles in the lower SEM) is fabricated in the vicinity of the resonator and capacitively coupled to the resonator.

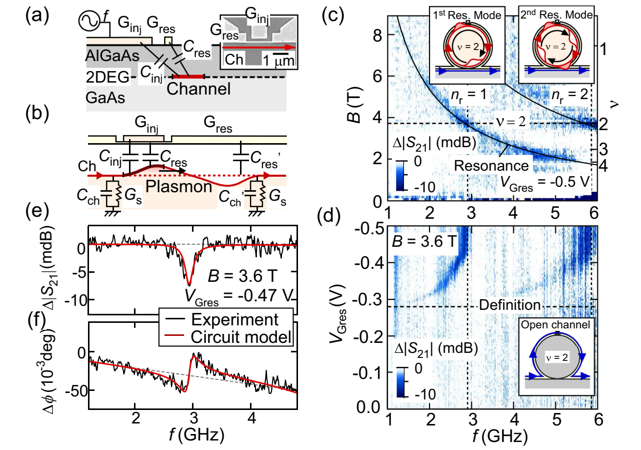

FIG. 2. (a) Schematic cross section of the edge channel and the injection gate G_{inj}. A top-view SEM picture is shown in the inset. (b) Distributed circuit model for the edge channel (Ch) with coupling capacitances, C_{ch}, C_{res}, and C_{inj} in the injection region, C'_{ch} and C'_{res} in the other region, and dissipative conductance G_s in both regions. (c) Transmission spectra $\Delta|S_{21}|(f, B)$ obtained at $V_{G\,res} = -0.5$ V. The right axis shows the filling factor ν. The resonant plasmon signals are seen in the blue regions for $n_r = 1$ and 2 with the charge density profiles illustrated in the insets. (d) $\Delta|S_{21}|(f, V_{G\,res})$ measured at $B = 3.6$ T. (e) The amplitude $\Delta|S_{21}|$ and (f) the phase $\Delta\phi$ obtained at $B = 3.6$ T and $V_{G\,res} = -0.47$ V. The red lines are calculated with distributed circuit model.

(2DEG) having an electron density of 1.8×10^{11} cm^{-2} (see Supplemental Material (SM) [37]). Under a magnetic field B perpendicular to the 2DEG, the plasmon resonator is defined by applying negative voltage $V_{G\,res}$ (< -0.28 V) to the ring-shaped gate G_{res} with perimeter $L = 126$ μm (the resonant frequency $f_0 \sim 3$ GHz at $\nu = 2$). The plasmon mode (charge density wave) can be excited by applying microwave voltage to the top electrode G_{inj} through the coplanar transmission line and with a capacitive coupling scheme as shown in Fig. 2(a). We investigate rf transmission coefficient S_{21} from port 1 to port 2 of the coplanar line to characterize the resonator. The plasmon resonance can be simulated by a distributed circuit model [37], as shown in Fig. 2(b). A gate defined DQD was formed in the vicinity of the plasmon resonator. A TLS can be defined by choosing a single level in each dot. The static energy bias ε and the tunneling coupling t_{12} of the DQD can be varied by tuning the gate voltages. The tunneling current I_d from the source (S) through the DQD to the drain (D) was measured with applying a source-drain voltage V_{sd}. The DQD is tuned in a weak tunnel coupling regime ($t_{12} \ll hf_0$), where clear PlAT is expected with the large permanent dipole moment. All measurements are performed at a temperature of ~85 mK.

First, we evaluate the plasmon resonator by measuring S_{21} with the resonator activated at negative $V_{G\,res}$, while other gates for the DQD were grounded. The resonance should appear in tiny change in $|S_{21}|$, which can be visible by subtracting the background signal $|S^0_{21}|$ obtained at $V_{G\,res} = 0$ V without forming the plasmon resonator. Figure 2(c) shows the subtracted spectra $\Delta|S_{21}| = |S_{21}| - |S^0_{21}|$ (in the decibel unit) as a function of frequency f and magnetic field B. The plasmon resonances are identified as negative peaks with $\Delta|S_{21}| < 0$ dB (the blue regions). The resonant frequency decreases monotonically with increasing B, which is the signature of the edge-magnetoplasmon mode [24]. Considering that the plasmon velocity $v = \sigma_{xy}/C_\Sigma$ is determined by the Hall conductance $\sigma_{xy} = \nu e^2/h$ and the channel capacitance C_Σ, the resonant frequency of the n_rth mode follows $f = n_r v/L$ [39,40]. This reproduces the resonant frequencies, as shown by the solid lines for $n_r = 1$ and 2 with $C_\Sigma = 0.21$ nF/m. This C_Σ is consistent with previous studies on gate-defined edge channels [28,41]. The observed multiple resonant modes clearly manifest the wave nature of the plasmons. The $n_r = 1$ resonance is significantly enhanced at $B \simeq 3.6$ T, where a $\nu = 2$ QH state is formed with negligible longitudinal resistance. The resonance signal weakens as ν deviates from 2, possibly due to the dissipation attributed to local disorders around the channel or in the bulk [23,42]. While charge and spin collective modes are anticipated at $\nu = 2$ [20], we focus on the charge (edge-magnetoplasmon) mode with large Z in this study.

The resonant frequency can be tuned electrostatically, as shown in the $V_{G\,res}$ dependence of $\Delta|S_{21}|$ at $B = 3.6$ T in Fig. 2(d). The resonant peaks for both $n_r = 1$ and 2 modes appear at sufficiently negative $V_{G\,res}$ below the definition voltage (~ -0.28 V) and show blueshifts with more negative $V_{G\,res}$. This frequency shifts can be understood

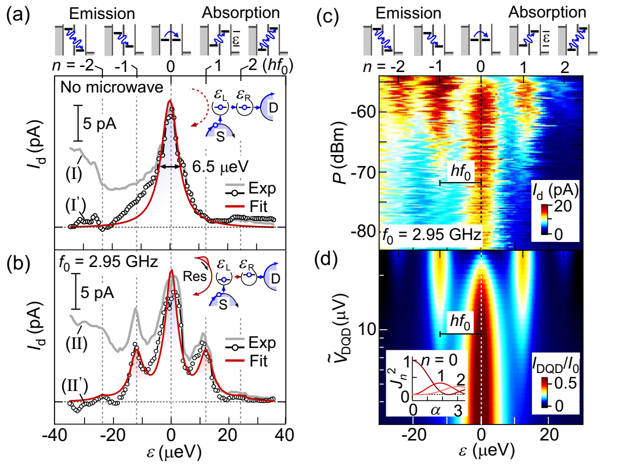

FIG. 3. (a),(b) Current spectra I_d measured (a) at $P = 0$ and (b) under plasmon irradiation at $P = -68$ dBm. Traces (I) and (II) show the raw data. Traces (I') and (II') are obtained by removing the background current and fitted with a theoretical model (the red lines). (c) Current spectra measured at $f_0 = 2.95$ GHz for various rf powers. Satellite peaks are observed up to $|n| = 2$ plasmons. (d) Calculated current spectra as a function of the ac voltage amplitude $\tilde{V}_{DQD}$ in the DQD. The inset shows the squared Bessel function $J_n^2(\alpha)$ of $\alpha = e\tilde{V}_{DQD}/hf_0$. The PlAT is illustrated in the upper insets of (a) and (c).

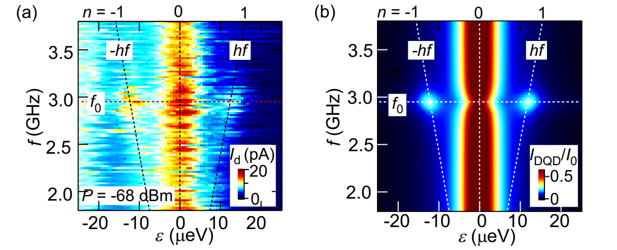

FIG. 4. (a) f dependence of current spectra measured at $P = -68$ dBm. Satellite peaks appear only at the plasmon resonant frequency $f_0 = 2.95$ GHz. (b) Calculated current spectra.

by considering the $V_{G\,res}$ dependence of the channel capacitance C_Σ, which decreases as $V_{G\,res}$ decreases and the edge channels move away from G_{res} [28]. In the following experiments for PlAT, we focus on the plasmon mode at $B = 3.6$ T and $V_{G\,res} = -0.47$ V, where the resonant frequency is $f_0 = 2.95$ GHz. The spectra of $\Delta|S_{21}|$ and $\Delta\phi = \arg(S_{21}) - \arg(S_{21}^0)$ at this condition are plotted in Figs. 2(e) and 2(f), respectively. They are well reproduced by a model calculation (the red lines, described in SM [37]) with quality factor $Q = 18$.

We now investigate the charge transport in the DQD with and without plasmon excitation. The DQD shows Coulomb charging energy of ~0.8 meV, single-particle energy spacing of ~140 μeV, and electrostatic coupling energy of ~86 μeV, as shown in SM [37]. Trace (I) in Fig. 3(a) shows the tunneling current I_d through particular energy levels, ε_L in the left dot and ε_R in the right dot, measured at zero microwave power ($P = 0$) and $V_{sd} = 400$ μV during the sweep of the gate voltages. The horizontal axis represents the energy detuning $\varepsilon = \varepsilon_R - \varepsilon_L$, where the detuning energy from the peak ($\varepsilon = 0$) is obtained from the gate voltage with a lever-arm factor. For clarity, the background current associated with other nearby levels is subtracted from trace (I) (See SM [37]), and the subtracted trace (I') with open circles can be fitted by using a Lorentzian curve (the red line) with full width of $w_{DQD} = 6.5$ μeV. The deviation at $\varepsilon < 0$ can be associated with the spontaneous phonon emission process [43].

The PlAT is observed under plasmon excitation, as shown by trace (II) of Fig. 3(b) obtained at $f_0 = 2.95$ GHz and microwave power $P = -68$ dBm estimated at the coplanar line (see SM) [37]. The background current from other levels is subtracted in trace (II'). The two distinct satellite peaks on both sides of the original peak are associated with absorption (the right peak at $\varepsilon > 0$) and emission (the left peak at $\varepsilon < 0$) of a single plasmon. This absorption tunneling is analogous to the photoelectric effect in which an electron is excited from a material by absorbing a photon. These peaks appear at $\varepsilon = \pm 12$ μeV, which coincides with the plasmon energy of $hf_0 = 12.2$ μeV. This means that a single plasmon can be removed from or added to the resonator by electron tunneling between the two dots. Significantly, these processes can be used for cQED applications.

The PlAT can be understood with the Tien-Gordon model [44], in which oscillating potential is applied across a tunneling barrier. In our case, the circulating plasmon waves with voltage amplitude $\tilde{V}_{res}$ in the resonator cause the oscillating potential with amplitude $e\tilde{V}_{DQD}$ between the two dots. This oscillating potential splits the eigenstates of the dots with detuning ε into a superposition of plasmon sidebands with energy $\varepsilon + nhf$ and amplitude $J_n(\alpha)$. The electron in the TLS is dressed with n plasmons in this picture. For the original current profile $I_0(\varepsilon)$ at $\tilde{V}_{DQD} = 0$, the current profile under the oscillating potential can be written as

$$I(\varepsilon) = \sum_n J_n^2(\alpha) I_0(\varepsilon + nhf_0), \quad n = 0, \pm 1, \pm 2, \ldots, \quad (1)$$

where the squared nth-order Bessel function of the first kind $J_n^2(\alpha)$ describes the probability of finding the system in the n-plasmon dressed state and thus provides the relative height of the nth satellite peak [45]. Here, $\alpha = e\tilde{V}_{DQD}/hf_0$ is the normalized amplitude of the oscillating potential. By using the Lorentzian profile $I_0(\varepsilon)$ fitted to the data in Fig. 3(a), the observed PlAT current profile can be reproduced with Eq. (1), as shown by the red line in Fig. 3(b) with $\alpha = 1.02$ ($e\tilde{V}_{DQD} = 12.4$ μeV).

Multiple-plasmon assisted tunneling is observed at higher microwave powers with the n-plasmon peak

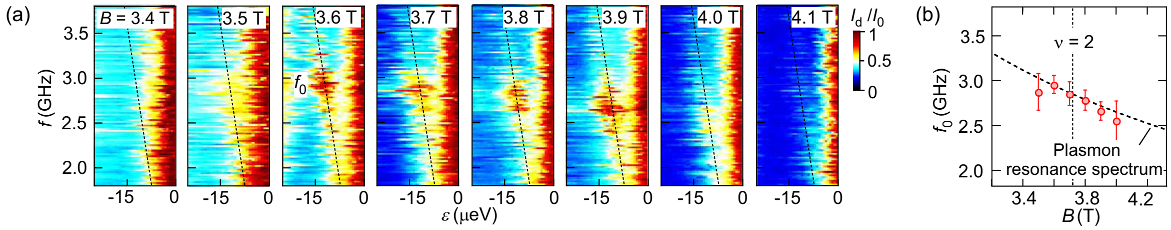

FIG. 5. (a) Current spectra measured at $B = 3.4\,\mathrm{T} - 4.1\,\mathrm{T}$. (b) B dependence of the resonant frequency f_0 extracted from the PlAT (the circles) and $\Delta|S_{21}|$ (the dashed line).

exhibiting nonlinear power dependence, as shown in Fig. 3(c); the two-plasmon absorption peak at $\varepsilon = 24\ \mu\mathrm{eV}$ and the two-plasmon emission peak at $\varepsilon = -24\ \mu\mathrm{eV}$ are seen at $P > -63$ dBm. The first-plasmon peak at $\varepsilon = \pm 12\ \mu\mathrm{eV}$ shows a maximum at $P = -57$ dBm and the zero-plasmon peak at $\varepsilon = 0$ vanishes at higher $P = -54$ dBm. These features are reproduced by Eq. (1) with the Bessel function, as shown in Fig. 3(d). All features can be understood with amplitude $J_n(\alpha)$ for n-plasmon dressed state. The observation of such a nonlinear optics regime for emergent edge plasmons is remarkable.

To justify that the signal is induced by the edge plasmons, its resonant characteristics are confirmed by measuring the current profiles at various frequencies, as shown in Fig. 4(a). The dashed lines describe the energy quantum $\varepsilon = \pm hf$ for frequency f. The PlAT is visible only at around $f_0 = 2.95$ GHz, and no signal is obtained at off-resonant conditions ($f \neq f_0$). The result is well reproduced by our simulation shown in Fig. 4(b), where $\tilde{V}_{\mathrm{DQD}}$ in Eq. (1) is assumed to be proportional to the Lorentzian profile of $\Delta|S_{21}|$ in Fig. 2(e). The resonant feature safely excludes possible artifacts, for example, associated with the long-range electrostatic crosstalk causing conventional photon-assisted tunneling [46,47].

We repeated similar experiments at several magnetic fields in the range of 3.4–4.1 T (corresponding ν between 2.2 and 1.8), as shown in Fig. 5(a), where the emission peak at $\varepsilon < 0$ is shown. The resonant frequency f_0 changes with B, as summarized in Fig. 5(b), in agreement with the $1/B$ dependence (the dashed line) extracted from the resonator characteristics of Fig. 2(c). The satellite peak in Fig. 5(a) is seen in the limited range of $B = 3.5$–4 T in agreement with the data in Fig. 2(c) (see SM [37]). The result unambiguously ensures that the QH plasmon mode is coupled to the DQD.

Having confirmed the coupling between the DQD and the edge plasmon mode that emerged from electrons, we shall discuss the feasibility of strong coupling regimes of cQED with edge plasmons. The vacuum Rabi splitting g normalized by the plasmon energy hf_0 determines the ultrastrong ($g/hf_0 \gtrsim 0.1$) and deep-strong ($g/hf_0 \gtrsim 1$) regimes [48,49]. For electric dipole coupling, it can be written as $g/hf_0 = \frac{1}{2}\zeta_{\mathrm{res}}\eta_{\mathrm{r-q}}\sin\theta_{\mathrm{qubit}}$ with three dimensionless factors [31]. The resonator factor $\zeta_{\mathrm{res}} = e\tilde{V}_{\mathrm{res}}/hf_0$ describes the normalized amplitude of the oscillating potential $e\tilde{V}_{\mathrm{res}}$ of the edge channel for single energy quantum hf_0 and is given by $\zeta_{\mathrm{res}} = \sqrt{Z(e^2/h)}$. Therefore, high-$Z$ resonators are highly desirable for larger $\tilde{V}_{\mathrm{res}}$ and ζ_{res} [50]. The edge plasmon resonator provides high $\zeta_{\mathrm{res}} = 1/\sqrt{2}$ at $\nu = 2$, and $\zeta_{\mathrm{res}} > 1$ in the fractional QH regimes. The qubit factor $\sin\theta_{\mathrm{qubit}} = 2t_{12}/\sqrt{\varepsilon^2 + 4t_{12}^2}$ describes the magnitude of the transition dipole moment, while $\cos\theta_{\mathrm{qubit}}$ describes that of the permanent dipole moment [47]. Whereas the present experiment was done at small $\sin\theta_{\mathrm{qubit}} \ll 1$ for demonstrating the PlAT associated with the permanent dipole moment, one can reach $\sin\theta_{\mathrm{qubit}} \simeq 1$ by tuning $t_{12} = \frac{1}{2}hf_0$ and $\varepsilon = 0$ with gate voltages. Therefore, the coupling factor $\eta_{\mathrm{r-q}} = \tilde{V}_{\mathrm{DQD}}/\tilde{V}_{\mathrm{res}}$ needs to be large for the strong coupling regimes.

$\eta_{\mathrm{r-q}}$ can be estimated from our data in the following way. First, we can relate $\tilde{V}_{\mathrm{res}}$ to the input microwave power P by using the capacitance model shown in Fig. 2(a). The channel can be divided into the injection region of length L_{inj} with finite capacitance C_{inj} and the other region of length $L - L_{\mathrm{inj}}$ with $C_{\mathrm{inj}} = 0$. The edge channel with conductance $\sigma_{xy} = 2e^2/h$ is also capacitively coupled to $\mathrm{G_{res}}$ with C_{res} and the rest (including the ground) with C_{ch} and dissipative conductance G_{s}, as shown in Fig. 2(b). The model successfully explains $\tilde{V}_{\mathrm{res}}$ measured with a quantum dot in our previous study [40]. The width and the height of the resonant peak in $\Delta|S_{21}|$ as well as $\tilde{V}_{\mathrm{res}}$ can be described by G_{s} and the product $C_{\mathrm{inj}}L_{\mathrm{inj}}$ in the limit of $L_{\mathrm{inj}} \ll L$. For the data at $P = -68$ dBm in Fig. 2(e), the profile can be fitted with $G_{\mathrm{s}} = 0.11$ S/m and $C_{\mathrm{inj}}L_{\mathrm{inj}} = 1.22$ fF, from which we deduce $\tilde{V}_{\mathrm{res}} \simeq 410\ \mu\mathrm{V}$ and the average number of plasmons $\langle n_{\mathrm{pl}}\rangle \simeq 2200$ at the resonant frequency. As we derived $\tilde{V}_{\mathrm{DQD}} = 12.4\ \mu\mathrm{V}$ at this condition, we estimate $\eta_{\mathrm{r-q}} \simeq 0.03$. This is reasonably high for the unoptimized device structure. As $\eta_{\mathrm{r-q}}$ strongly depends on the device geometry, we expect to reach $\eta_{\mathrm{r-q}} \gtrsim 0.1$ by placing the DQD closer to the resonator. Therefore, the ultrastrong regime at $g/hf_0 \gtrsim 0.1$ may be feasible with the scheme potentially.

Another important condition to reach the strong coupling regimes is that the energy loss rates κ of the resonator and γ of the qubit must be smaller than g. If the resonant line widths in the present measurements were determined by these dissipations, we estimate the upper bounds of $\kappa/hf_0 \simeq 1/Q \simeq 0.06$ and $\gamma/hf_0 \simeq w_{\mathrm{DQD}}/hf_0 \simeq 0.5$. The strong coupling regimes are expected by improving electrostatic environment of the edge channel for κ [35] and qubit environment for γ [51,52]. These crude estimations encourage us to study cQED with edge plasmons.

In summary, we have demonstrated PlAT in a hybrid quantum system of an edge-plasmon resonator and a DQD. Tunneling with absorption and emission of plasmon quanta manifests quantum properties of emergent plasmons in the quantum Hall regime. The plasmon-electron coupling with the high-impedance plasmon mode is attractive for studying strong coupling regimes of cQED. Overall, our study provides a foundation for combining the plasmons as topological quantum quasiparticles with quantum information devices. This integration makes the system particularly appealing for those new functionalities based on the high-impedance chiral mode.

The authors thank T. Hata and W. G. van der Wiel for their beneficial discussions. This study was supported by the Grants-in-Aid for Scientific Research Grants No. JP19H05603, No. JP24K06915, and JST PRESTO Grant No. JPMJPR225C and the TokyoTech-ARIM (Advanced Research Infrastructure for Materials and Nanotechnology) project.

*Contact author: lin.c.ad@m.titech.ac.jp

[1] C. Grenier, R. Hervé, G. Fève, and P. Degiovanni, Electron quantum optics in quantum Hall edge channels, Mod. Phys. Lett. B **25**, 1053 (2011).

[2] E. Bocquillon, V. Freulon, F. D. Parmentier, J. M. Berroir, B. Plaçais, C. Wahl, J. Rech, T. Jonckheere, T. Martin, C. Grenier, D. Ferraro, P. Degiovanni, and G. Fève, Electron quantum optics in ballistic chiral conductors, Ann. Phys. (Berlin) **526**, 1 (2014).

[3] T. Fujisawa, Nonequilibrium charge dynamics of Tomonaga-Luttinger liquids in quantum Hall edge channels, Ann. Phys. (Berlin) **2022**, 2100354 (2022).

[4] E. Bocquillon, V. Freulon, J. M. Berroir, P. Degiovanni, B. Plaçais, A. Cavanna, Y. Jin, and G. Fève, Coherence and indistinguishability of single electrons emitted by independent sources, Science **339**, 1054 (2013).

[5] J. D. Fletcher, W. Park, S. Ryu, P. See, J. P. Griffiths, G. A. C. Jones, I. Farrer, D. A. Ritchie, H.-S. Sim, and M. Kataoka, Time-resolved Coulomb collision of single electrons, Nat. Nanotechnol. **18**, 727 (2023).

[6] N. Ubbelohde, L. Freise, E. Pavlovska, P. G. Silvestrov, P. Recher, M. Kokainis, G. Barinovs, F. Hohls, T. Weimann, K. Pierz, and V. Kashcheyevs, Two electrons interacting at a mesoscopic beam splitter, Nat. Nanotechnol. **18**, 733 (2023).

[7] T. Ota, S. Akiyama, M. Hashisaka, K. Muraki, and T. Fujisawa, Spectroscopic study on hot-electron transport in a quantum Hall edge channel, Phys. Rev. B **99**, 085310 (2019).

[8] J. Wang, H. Edlbauer, A. Richard, S. Ota, W. Park, J. Shim, A. Ludwig, A. D. Wieck, H.-S. Sim, M. Urdampilleta, T. Meunier, T. Kodera, N.-H. Kaneko, H. Sellier, X. Waintal, S. Takada, and C. Bäuerle, Coulomb-mediated antibunching of an electron pair surfing on sound, Nat. Nanotechnol. **18**, 721 (2023).

[9] R. H. Rodriguez, F. D. Parmentier, D. Ferraro, P. Roulleau, U. Gennser, A. Cavanna, M. Sassetti, F. Portier, D. Mailly, and P. Roche, Relaxation and revival of quasiparticles injected in an interacting quantum Hall liquid, Nat. Commun. **11**, 2426 (2020).

[10] L. Freise, T. Gerster, D. Reifert, T. Weimann, K. Pierz, F. Hohls, and N. Ubbelohde, Trapping and counting ballistic nonequilibrium electrons, Phys. Rev. Lett. **124**, 127701 (2020).

[11] K. Suzuki, T. Hata, Y. Sato, T. Akiho, K. Muraki, and T. Fujisawa, Non-thermal Tomonaga-Luttinger liquid eventually emerging from hot electrons in the quantum Hall regime, Commun. Phys. **6**, 103 (2023).

[12] T. Jullien, P. Roulleau, B. Roche, A. Cavanna, Y. Jin, and D. C. Glattli, Quantum tomography of an electron, Nature (London) **514**, 603 (2014).

[13] R. Bisognin, A. Marguerite, B. Roussel, M. Kumar, C. Cabart, C. Chapdelaine, A. Mohammad-Djafari, J.-M. Berroir, E. Bocquillon, B. Plaçais, A. Cavanna, U. Gennser, Y. Jin, P. Degiovanni, and G. Fève, Quantum tomography of electrical currents, Nat. Commun. **10**, 3379 (2019).

[14] A. M. Chang, Chiral Luttinger liquids at the fractional quantum Hall edge, Rev. Mod. Phys. **75**, 1449 (2003).

[15] X. G. Wen, Electrodynamical properties of gapless edge excitations in the fractional quantum Hall states, Phys. Rev. Lett. **64**, 2206 (1990).

[16] I. Grodnensky, D. Heitmann, and K. von Klitzing, Nonlocal dispersion of edge magnetoplasma excitations in a two-dimensional electron system, Phys. Rev. Lett. **67**, 1019 (1991).

[17] E. Bocquillon, V. Freulon, J. M. Berroir, P. Degiovanni, B. Plaçais, A. Cavanna, Y. Jin, and G. Fève, Separation of neutral and charge modes in one-dimensional chiral edge channels, Nat. Commun. **4**, 1839 (2013).

[18] H. Inoue, A. Grivnin, N. Ofek, I. Neder, M. Heiblum, V. Umansky, and D. Mahalu, Charge fractionalization in the integer quantum Hall effect, Phys. Rev. Lett. **112**, 166801 (2014).

[19] H. Kamata, N. Kumada, M. Hashisaka, K. Muraki, and T. Fujisawa, Fractionalized wave packets from an artificial Tomonaga-Luttinger liquid, Nat. Nanotechnol. **9**, 177 (2014).

[20] M. Hashisaka, N. Hiyama, T. Akiho, K. Muraki, and T. Fujisawa, Waveform measurement of charge- and spin-density wavepackets in a chiral Tomonaga-Luttinger liquid, Nat. Phys. **13**, 559 (2017).

[21] M. Hashisaka, T. Jonckheere, T. Akiho, S. Sasaki, J. Rech, T. Martin, and K. Muraki, Andreev reflection of fractional quantum Hall quasiparticles, Nat. Commun. **12**, 2749 (2021).

[22] M. Hashisaka and T. Fujisawa, Tomonaga-Luttinger-liquid nature of edge excitations in integer quantum Hall edge channels, Rev. Phys. **3**, 32 (2018).

[23] R. C. Ashoori, H. L. Stormer, L. N. Pfeiffer, K. W. Baldwin, and K. West, Edge magnetoplasmons in the time domain, Phys. Rev. B **45**, 3894 (1992).

[24] V. I. Talyanskii, A. V. Polisski, D. D. Arnone, M. Pepper, C. G. Smith, D. A. Ritchie, J. E. Frost, and G. A. C. Jones, Spectroscopy of a two-dimensional electron gas in the

quantum-Hall-effect regime by use of low-frequency edge magnetoplasmons, Phys. Rev. B **46**, 12427 (1992).
[25] N. Kumada, P. Roulleau, B. Roche, M. Hashisaka, H. Hibino, I. Petković, and D. C. Glattli, Resonant edge magnetoplasmons and their decay in graphene, Phys. Rev. Lett. **113**, 266601 (2014).
[26] N. Hiyama, M. Hashisaka, and T. Fujisawa, An edge-magnetoplasmon Mach-Zehnder interferometer, Appl. Phys. Lett. **107**, 143101 (2015).
[27] H. Bartolomei, R. Bisognin, H. Kamata, J.-M. Berroir, E. Bocquillon, G. Ménard, B. Plaçais, A. Cavanna, U. Gennser, Y. Jin, P. Degiovanni, C. Mora, and G. Fève, Observation of edge magnetoplasmon squeezing in a quantum Hall conductor, Phys. Rev. Lett. **130**, 106201 (2023).
[28] H. Kamata, T. Ota, K. Muraki, and T. Fujisawa, Voltage controlled group velocity of edge magnetoplasmon in the quantum Hall regime, Phys. Rev. B **81**, 085329 (2010).
[29] S. Bosco, D. P. DiVincenzo, and D. J. Reilly, Transmission lines and metamaterials based on quantum Hall plasmonics, Phys. Rev. Appl. **12**, 014030 (2019).
[30] M. H. Devoret, S. Girvin, and R. Schoelkopf, Circuit-QED: How strong can the coupling between a Josephson junction atom and a transmission line resonator be?, Ann. Phys. (Amsterdam) **16**, 767 (2007).
[31] L. Childress, A. S. Sørensen, and M. D. Lukin, Mesoscopic cavity quantum electrodynamics with quantum dots, Phys. Rev. A **69**, 042302 (2004).
[32] C. Altimiras, O. Parlavecchio, P. Joyez, D. Vion, P. Roche, D. Esteve, and F. Portier, Tunable microwave impedance matching to a high impedance source using a Josephson metamaterial, Appl. Phys. Lett. **103**, 212601 (2013).
[33] A. Stockklauser, P. Scarlino, J. V. Koski, S. Gasparinetti, C. K. Andersen, C. Reichl, W. Wegscheider, T. Ihn, K. Ensslin, and A. Wallraff, Strong coupling cavity QED with gate-defined double quantum dots enabled by a high impedance resonator, Phys. Rev. X **7**, 011030 (2017).
[34] P. Scarlino, J. H. Ungerer, D. J. van Woerkom, M. Mancini, P. Stano, C. Müller, A. J. Landig, J. V. Koski, C. Reichl, W. Wegscheider, T. Ihn, K. Ensslin, and A. Wallraff, *In situ* tuning of the electric-dipole strength of a double-dot charge qubit: Charge-noise protection and ultrastrong coupling, Phys. Rev. X **12**, 031004 (2022).
[35] S. Bosco and D. P. DiVincenzo, Transmission lines and resonators based on quantum Hall plasmonics: Electromagnetic field, attenuation, and coupling to qubits, Phys. Rev. B **100**, 035416 (2019).
[36] Samuel J. Elman, Stephen D. Bartlett, and Andrew C. Doherty, Long-range entanglement for spin qubits via quantum Hall edge modes, Phys. Rev. B **96**, 115407 (2017).
[37] See Supplemental Material at http://link.aps.org/supplemental/10.1103/PhysRevLett.133.036301 for experimental details transmission line and device characteristics, circuit model of the plasmon resonator, and simulations, which includes Ref. [38].
[38] N. C. van der Vaart, S. F. Godijn, Y. V. Nazarov, C. J. P. M. Harmans, J. E. Mooij, L. W. Molenkamp, and C. T. Foxon, Resonant tunneling through two discrete energy states, Phys. Rev. Lett. **74**, 4702 (1995).
[39] M. Hashisaka, H. Kamata, N. Kumada, K. Washio, R. Murata, K. Muraki, and T. Fujisawa, Distributed-element circuit model of edge magnetoplasmon transport, Phys. Rev. B **88**, 235409 (2013).
[40] T. Ota, M. Hashisaka, K. Muraki, and T. Fujisawa, Electronic energy spectroscopy of monochromatic edge magnetoplasmons in the quantum Hall regime, J. Phys. Condens. Matter **30**, 345301 (2018).
[41] C. J. Lin, M. Hashisaka, T. Akiho, K. Muraki, and T. Fujisawa, Quantized charge fractionalization at quantum Hall *Y* junctions in the disorder dominated regime, Nat. Commun. **12**, 131 (2021).
[42] C. J. Lin, M. Hashisaka, T. Akiho, K. Muraki, and T. Fujisawa, Time-resolved investigation of plasmon mode along interface channels in integer and fractional quantum Hall regimes, Phys. Rev. B **104**, 125304 (2021).
[43] T. Fujisawa, T. H. Oosterkamp, W. G. van der Wiel, B. W. Broer, R. Aguado, S. Tarucha, and L. P. Kouwenhoven, Spontaneous emission spectrum in double quantum dots, Science **282**, 932 (1998).
[44] P. K. Tien and J. R. Gordon, Multiphoton process observed in the interaction of microwave fields with the tunneling between superconductor films, Phys. Rev. **129**, 647 (1963).
[45] T. H. Stoof and Yu. V. Nazarov, Time-dependent resonant tunneling via two discrete states, Phys. Rev. B **53**, 1050 (1996).
[46] T. H. Oosterkamp, T. Fujisawa, W. G. van der Wiel, K. Ishibashi, R. V. Hijman, S. Tarucha, and L. P. Kouwenhoven, Microwave spectroscopy of a quantum-dot molecule, Nature (London) **395**, 873 (1998).
[47] W. G. van der Wiel, S. De Franceschi, J. M. Elzerman, T. Fujisawa, S. Tarucha, and L. P. Kouwenhoven, Electron transport through double quantum dots, Rev. Mod. Phys. **75**, 1 (2002).
[48] S. Haroche and J. M. Raimond, *Exploring the Quantum: Atoms, Cavities, and Photons* (Oxford University Press, New York, 2006).
[49] A. Blais, A. L. Grimsmo, S. M. Girvin, and A. Wallraff, Circuit quantum electrodynamics, Rev. Mod. Phys. **93**, 025005 (2021).
[50] A. Blais, R. S. Huang, A. Wallraff, S. M. Girvin, and R. J. Schoelkopf, Cavity quantum electrodynamics for superconducting electrical circuits: An architecture for quantum computation, Phys. Rev. A **69**, 062320 (2004).
[51] T. Hayashi, T. Fujisawa, H. D. Cheong, Y. H. Jeong, and Y. Hirayama, Coherent manipulation of electronic states in a double quantum dot, Phys. Rev. Lett. **91**, 226804 (2003).
[52] G. Shinkai, T. Hayashi, T. Ota, and T. Fujisawa, Correlated coherent oscillations in coupled semiconductor charge qubits, Phys. Rev. Lett. **103**, 056802 (2009).